Hydroxyl Radical Self-Recombination Reaction and Absorption Spectrum in Water Up to 350 °C

Ireneusz Janik and David M. Bartels*

University of Notre Dame, Radiation Laboratory, Notre Dame, Indiana 46556

Charles D. Jonah

Chemistry Division, Argonne National Laboratory, Argonne, Illinois 60439

Received: September 13, 2006; In Final Form: January 5, 2007

The rate constant for the self-recombination of hydroxyl radicals (•OH) in aqueous solution giving H_2O_2 product has been measured from 150 to 350 °C by direct measurement of the •OH radical transient optical absorption at 250 nm. The values of the rate constant are smaller than previously predicted by extrapolation to the 200−350 °C range and show virtually no change in this range. In combining these measurements with previous results, the non-Arrhenius behavior can be well described in terms of the Noyes equation $k_{obs}^{-1} = k_{act}^{-1} + k_{diff}^{-1}$, using the diffusion-limited rate constant k_{diff} estimated from the Smoluchowski equation and an activated barrier rate k_{act} nearly equal to the gas-phase high-pressure limiting rate constant for this reaction. The aqueous •OH radical spectrum between 230 and 320 nm is reported up to 350 °C. A weak band at 310 nm grows in at higher temperature, while the stronger band at 230 nm decreases. An isosbestic point appears near 305 nm. We assign the 230 nm band to hydrogen-bonded •OH radical, and the 310 nm band is assigned to "free" •OH. On the basis of the spectrum change relative to room temperature, over half of the •OH radicals are in the latter form at 350 °C.

I. Introduction

The hydroxyl radical (•OH) is arguably the most important free radical species in oxidation processes of technological importance. It is a primary chain carrier in flame chemistry,[1] and the main actor in water-solvent-based "advanced oxidation processes".[2] It is a primary product of water radiolysis with ionizing radiation,[3] photolysis with UV photons,[4] or even bubble collapse in sonolysis.[5] The importance of the species has stimulated many, many studies of its reactions in the gas phase[6] and in aqueous solution.[7−10] To our knowledge, however, few connections have been established between the reaction rates of •OH in the gas phase and in condensed phases. Can we use gas-phase and ab initio results to accurately predict reaction rates in solution, and particularly water? The present study makes the first direct connection between gas-phase and aqueous solution reaction rates for the important self-recombination of •OH radicals, giving hydrogen peroxide product.

In water-cooled nuclear power plants, •OH self-recombination is a primary source of corrosive hydrogen peroxide and oxygen molecules. The need to model radiation-induced chemistry in reactor heat transport piping has stimulated the present study. In particular, one would like to predict feasibility of reactors cooled with supercritical water (SCW), because this can significantly improve economics of the power generation over present-day reactors.[11,12] Recent studies on SCW-cooled nuclear reactors involve still unresolved questions about the water radiolysis mechanism and the water radiolysis product yields at elevated pressures and temperatures. Because of their relevance to the corrosion issue, the reactions

$$^{\bullet}OH + {}^{\bullet}OH \rightarrow H_2O_2 \quad (1)$$

and

$$^{\bullet}OH + H_2O_2 \rightarrow HO_2^{\bullet} + H_2O \quad (2)$$

received significant attention.[13]

Temperature studies of reaction 1 in the gas phase cover a wide range of conditions beginning from the low-pressure limit,[14] through the falloff range, and to high-pressure limiting values[15,16] ($k_{1,\infty}$). Unexpected behavior of the simple association reaction of two •OH radicals was the subject of several theoretical studies.[17−20] From ab initio calculations of the potential energy surface for H_2O_2 it becomes clear that during the approach of two •OH radicals, at first dipole−dipole forces are dominant, and a weakly hydrogen-bonded HOHO metastable intermediate forms. This intermediate isomerizes over a small potential barrier into HOOH to finally form hydrogen peroxide in its singlet electronic ground state. Besides the ground state there are electronically excited potentials that interact with the ground-state potential in a complicated manner. To investigate whether excited electronic states contribute to the kinetic behavior, Fulle et al.[16] performed measurements of high-pressure limiting rate constants for reaction 1, $k_{1,\infty}$. In the temperature range 200−700 K they measured saturated laser-induced fluorescence (SLIF) of •OH radicals in a helium bath gas up to 100 bar. In the conclusion of their studies they reported no temperature effect between 200 and 400 K on the high-pressure limiting rate $k_{1,\infty}$, and even a slight negative temperature effect on the rate coefficients between 400 and 700 K. At that time

* To whom correspondence should be addressed. E-mail: bartels@hertz.rad.nd.edu. Phone: (574) 631-5561. Fax: (574) 631-8068.

10.1021/jp065992v CCC: $37.00
Published on Web 02/20/2007

the negative temperature effect was explained as underestimation of the high-pressure limit due to an insufficient range of bath gas pressures used in the experiment. However, in a subsequent review about quantitative analysis of association reactions in the atmosphere, Troe[21] presented detailed analysis of the temperature dependence of capture rate constants for reaction 1 and concluded that reaction 1 should have a very weak negative temperature coefficient over the range 30−1300 K.

Knowledge of the gas-phase high-pressure limiting rate constants can benefit the analysis of partially diffusion-limited condensed-phase reaction rates when observed rate constants follow the Noyes equation:[13,22]

$$k_{obs}^{-1} = k_{act}^{-1} + k_{diff}^{-1} \quad (3)$$

Here k_{obs} is the observed rate constant in the condensed phase at a given temperature, k_{act} is the hypothetical limiting reaction rate in absence of a diffusional concentration gradient,[23] and k_{diff} is a diffusion-limited reaction rate determined on the basis of the Smoluchowski equation:

$$k_{diff} = \beta\sigma 4\pi RD \quad (4)$$

where $D = D_a + D_b$ is the relative diffusion coefficient of reactants a and b, R is the reaction distance, β is a spin statistics factor, and σ is $^1/_2$ for identical reactants but unity otherwise.

The earlier temperature studies of reaction 1 up to 200 °C were performed by measuring the decay of •OH radical transient absorption in the deep UV.[24−26] The latest work by Elliot et al.[26] reports a rate constant of 4.0×10^9 M^{-1} s^{-1} at 25 °C and average activation energy of 7.0 kJ mol^{-1}. In a later review, Elliot[13] concluded that either an Arrhenius equation or the Noyes equation (3) describes the data to within the experimental error, and essentially the same value is given by either equation when extrapolated to 300 °C (within 10%). This extrapolation suggests a slight increase of the reaction 1 rate constant over the range of temperature 200−350 °C[13].

In the present investigation, the •OH radical recombination has been studied at temperatures up to 350 °C using pulse radiolysis. The system chosen to study this reaction was N_2O-saturated water. Radiolysis produces mainly •OH radical and e^-_{aq}, with a smaller amount of H• atom.[3,7] In the presence of N_2O, solvated electrons are quickly converted to •OH radicals via reaction 5, giving the desired •OH radical as ca. 90% of the

$$e^-_{aq} + N_2O + H_2O \rightarrow {}^{\bullet}OH + N_2 + OH^- \quad (5)$$

total at room temperature. To extract second-order recombination rate constants, an absolute concentration scale must be established via the free radical extinction coefficients. In the sections below we describe first the work required to establish the extinction coefficients at high temperature, and then the procedure followed in analyzing the rate constants. We discuss the changes in the •OH radical spectrum with temperature and interpret the recombination rates by comparison with the gas-phase results.

II. Experimental Section

At wavelengths 250 nm and below, microsecond kinetic spectrophotometry becomes difficult because the intensities of the available analyzing light sources are low, and optical transmission losses are high, both from the sapphire of the SCW cell windows and from the water absorption in this region at higher temperatures.[27] These adverse conditions lead to a high photodetector shot noise level, poor spectral purity due to scattering of the abundant longer-wavelength light in a single monochromator, and interference from the intense Cerenkov light emitted in the UV region. To overcome these problems in the present work, an optical system was set up to provide optimum performance in the UV (Figure 1).

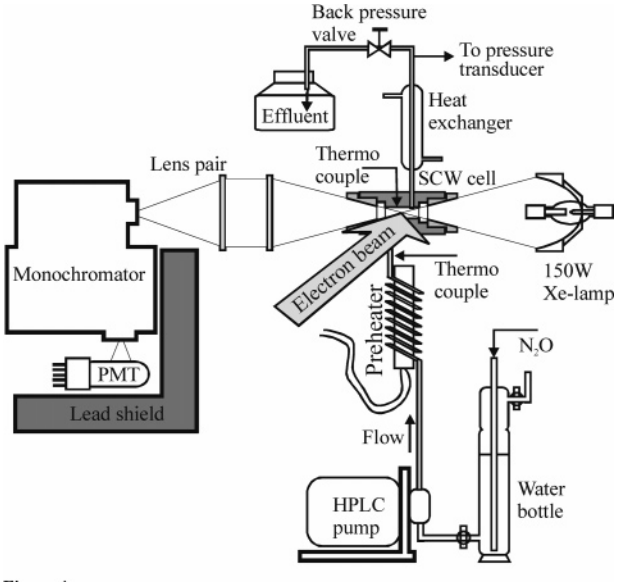

Figure 1. Experimental setup for measuring high-temperature pressurized water UV transient absorption.

The light source used was an XBO 150 W/S xenon arc lamp (Osram G.m.b.H., Germany). The arc was intensified approximately 30-fold using a transistorized pulser designed to produce a flat-topped 300 μs light pulse. By means of a magnesium fluoride coated parabolic reflector (PTI-033-0008-A), the arc was imaged through the absorption cell and suprasil lens pair onto the entrance slit of a double monochromator (DH-10, Instruments, SA. Inc.). Gratings with 1200 groove/mm blazed for maximum efficiency at 250 nm were used; the measured scattered light at 225 nm was less than 0.3%. The entrance, intermediate, and exit slit widths were set to 0.25, 1, and 2 mm, respectively, giving a half-maximum intensity bandwidth of 4.8 nm (for all slits being 2 mm, the bandwidth increases to 8 nm). The light emerging from the monochromator exit slit was directed onto the photocathode of a solar-blind photomultiplier (Hamamatsu R1319).

Pulse radiolysis/transient absorption experiments were carried out using 4−20 ns pulses from the Argonne Chemistry Division's 20 MeV electron linac accelerator. A lead shield was constructed to reduce the X-ray interference on the photomultiplier operation. The average dose per pulse was monitored by charge integration on a thick copper shutter that could be lowered in front of the cell. The sample cell, flow system, and basic experimental setup and characteristics were described in previous publications.[28,29] To improve the signal-to-noise ratio, signals were averaged over 30 consecutive traces. Due to transient absorption of sapphire windows after the pulse of electrons (see section IIIB), blank traces for a given dose and temperature were collected in the empty cell purged with flowing argon gas. These blank traces were subtracted from the corresponding traces collected for aqueous samples at the same temperature.

Samples were prepared by saturating water with N_2O (AGA Gas, Ultra-High Purity grade) at ambient conditions resulting in a final concentration of N_2O of 2.5×10^{-2} molal (m). The solution was then pumped with the high-pressure liquid chromatography pump at flow rates from 1.6 to 2.0 mL/min

TABLE 1: *G* Values and Extinction Coefficients for Primary Absorbing Species Applied in Data Analysis

	G(X) (mol J^{-1}) × 10^{-7}			ϵ (dm^3 mol^{-1} cm^{-1})			
temp (°C)	e^-_{aq}	H•	•OH	•OH	H•	HO_2•/O_2•$^-$	H_2O_2
25	2.86	0.57	2.90	535	30	1880	22
150	3.32	0.71	3.82	465	57	1810	39
200	3.43	0.85	4.03	425	68	1760	45
225	3.48	0.93	4.13	390	73	1523	48
250	3.50	1.04	4.24	364	78	1415	52
275	3.49	1.20	4.35	331	84	1262	55
300	3.44	1.43	4.46	296	89	1082	58
325	3.33	1.77	4.59	260	95	871	62
350	3.13	2.25	4.73	224	100	720	65

through the preheater and then into the high-temperature, corrosion-resistant, hastelloy C-276 cell.[30] Auxiliary cartridge heaters compensated any heat loss inside the insulated cell housing. To minimize light scattering, the temperature of the solution introduced to the cell was kept within 0.5 °C of the destination set point temperature. All the measurements were performed at the same pressure 250 ± 0.2 bar.

III. Results

We present results that were obtained after many iterations of fitting both kinetics and spectra of the several species involved. First we present the spectra and extinction coefficients and describe how they were extracted. Then we describe the salient kinetics observations and the analysis approach that was followed. Finally, we show the rate constants needed to fit the kinetics.

A. Extinction Coefficients. *•OH.* The prompt (ca. 100−120 ns after radiolysis) UV transient radical spectrum ($G \times \epsilon$) was measured in N_2O saturated water at ambient temperature as well as at higher temperatures. This spectrum is dominated by •OH absorption but includes contributions from H• atoms, H_2O_2, and HO_2•/O_2•$^-$. The G values for •OH and H• were calculated on the basis of data reported previously by Lin et al.[31] up to 350 °C. From the total G(•OH + e^-_{aq} + H•) reported by Lin et al. we subtracted the sum of G(H•) and $G(e^-_{aq})$ determined in our laboratory from gas product analysis in irradiated N_2O-saturated aqueous solutions of phenol and EtOH-d_6.[32] These numbers are tabulated in Table 1. The G values of H_2O_2 were taken from γ radiolysis experiments reported up to 300 °C and were extrapolated up to 350 °C.[13] The measured absorption at room temperature was corrected for H• atom absorption using the spectrum reported by Nielsen et al.[33] At higher temperatures spectra were corrected for H• atom absorption assuming the same red shift as was found for the absorption edge of water itself (see below).[27] We also made a small correction for H_2O_2 absorption[33,34] assuming that its spectrum also red shifts with the temperature. Figure 2 shows resulting spectra of •OH radicals in the range of 30−350 °C. All spectra were obtained at the same dose within ±5% deviation in day to day experiments. The spectrum obtained at room temperature agrees very well with the spectra recorded previously by Nielsen et al.[33] and others.[9,35] With an increase in temperature we observed an apparent decrease of absorption at the wavelength of our interest, i.e., 250 nm. However, above 300 °C we observed a sudden increase of the absorption at 250 nm and shorter wavelengths. After correction for the red-shifting H• atom absorption, it became obvious that with the increase of temperature, •OH absorption continuously decreases at the wavelength of interest. Therefore we collected also $G \times \epsilon$ values at 250 nm for all remaining temperatures in the experimental range. The change of extinction coefficient at 250 nm is shown in Figure 2 (inset). The values of •OH radical extinction coefficient are also summarized in Table 1.

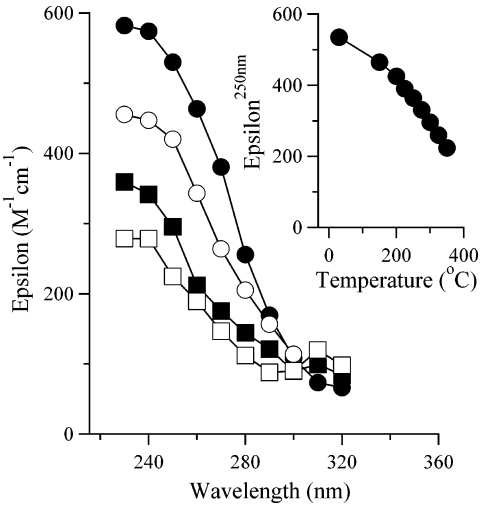

Figure 2. •OH radical spectrum change vs temperature: (●) 30 °C; (○) 200 °C; (■) 300 °C; (□) 350 °C. Extinction coefficients were calculated from measured $G \times \epsilon$ on the basis of G(•OH) for the given temperature as described in the text. Inset: changes of ϵ^{250} nm for •OH radicals vs temperature.

H•. The room-temperature H• atom extinction coefficient at 250 nm is less than or equal to 30 M^{-1} cm^{-1}. [33] The shape of the spectrum is known to remain the same up to 250 °C, essentially an exponential decrease toward the red.[36] If the amplitude changes with temperature, its contribution to observed absorption is expected to be more pronounced above 300 °C where the ratio G(H•)/G(•OH) increases. At 350 °C the H• atom yield reaches up to 30% of the total yield of •OH radicals in our system, and uncertainty of its extinction coefficient can impact the measured rate of reaction 1. This absorption has been identified as a red shift of those water molecules in the immediate solvation shell of the H atom.[33] The absorption edge of water itself shifts to the red by 0.5 eV from room temperature to 350 °C,[27] and a similar shift may be expected for the H atom absorption. If a 0.5 eV shift occurs, the H• atom extinction coefficient will reach a value of about 190 M^{-1} cm^{-1} at 250 nm (at room temperature this is the extinction coefficient at 230 nm[33]). The values between room temperature and 350 °C were scaled with the temperature according to this assumption and are summarized in Table 1.

H_2O_2. Hydrogen peroxide, whose extinction coefficient at 250 nm is roughly 22 M^{-1} cm^{-1},[33,34] needs to be included in the fitting as it is a final product of •OH decay. The apparent increase of the relative final absorption (see section B) implied that the hydrogen peroxide UV spectrum also becomes more intense or shifts to the red at elevated temperature. This spectrum is very difficult to measure accurately at elevated temperature because hydrogen peroxide catalytically decomposes on metal oxide surfaces. We estimate the H_2O_2 extinction coefficient by assuming a red shift of the H_2O_2 absorption spectrum with temperature similar to that of water. The result is consistent with the magnitude of the product absorption at 250 nm. The values are summarized in Table 1. It has subsequently been pointed out to us that the long-wavelength (longer than 230 nm) tail of H_2O_2 absorbance in the gas phase does increase substantially with temperature,[37] and this may also contribute to the liquid-phase result.

HO_2•/O_2•$^-$. As a product of reaction 2, the effective extinction coefficient of this radical at neutral pH was expected to be very important for data analysis. We have measured the effective

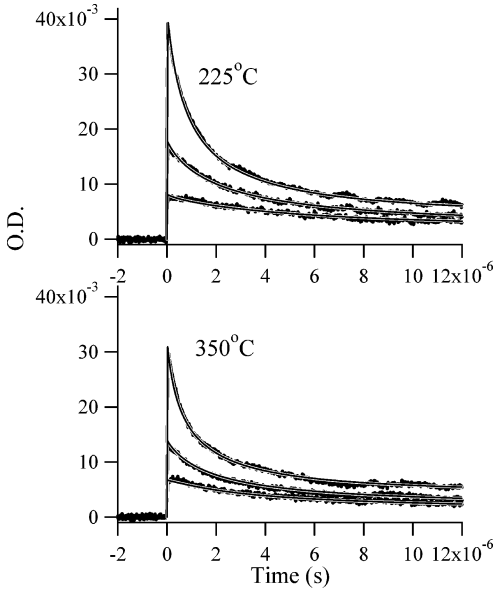

Figure 3. Comparison of •OH radical 250 nm absorption decay profiles recorded at 225 °C (upper) and 350 °C (lower) with global fit traces superimposed.

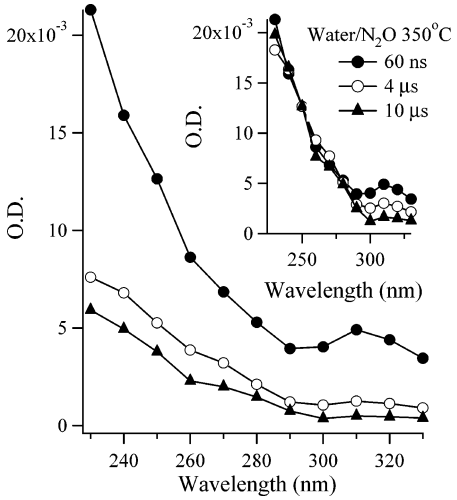

Figure 4. UV absorption spectral time evolution for N_2O aqueous solution after a 10 ns electron pulse at 350 °C: (●) 60 ns after electron pulse; (○ 2 μs after electron pulse; (▲) 10 μs after electron pulse. Inset: same spectra normalized at 250 nm. The relative absorption decrease is especially pronounced near 310 nm.

extinction coefficient for $HO_2^{\bullet}/O_2^{\bullet-}$ in the temperature range 30−350 °C in neutral water containing 5.0×10^{-2} *m* H_2 and 6.5×10^{-4} *m* of oxygen.[38] The change of effective extinction coefficient at 250 nm with temperature is summarized in Table 1. With the increase of the temperature we observed gradual decrease of the extinction coefficient from roughly 1880 to 720 M^{-1} cm^{-1}. This is the result of the shifting from ionic form to protonated form, as the pK_a value of the radical is expected to change from 4.8 at room temperature to about 7.05 at 350 °C.[39] (This room-temperature value is roughly 15% lower than the number reported by Bielski et. al[40] at pH = 6 but agrees with the later Elliot and Buxton observations.[41]) More detailed analysis of $HO_2^{\bullet}/O_2^{\bullet-}$ spectral changes with temperature have been presented in a paper dealing with the reaction of H• with O_2.[38]

B. Data Analysis. Initially, we analyzed •OH decay traces using the simplest model possible. We applied just the two reactions (1) and (2), and we were able to achieve reasonably good global fitting for data collected in the entire experimental temperature range. The first observation resulting from collected data was that on increasing temperature to 350 °C we saw a gradual increase in the product absorption after completion of reaction 1. A comparison of signals collected at 225 and 350 °C is presented in Figure 3. With an increase of the temperature the ratio between initial and final signal amplitude decreases, suggesting that either the H_2O_2 product extinction coefficient increases with temperature or the rate constant for reaction (2) is higher than extrapolated from data[42] collected in the temperature range 25−150 °C. (The •OH radical spectrum was already corrected for temperature, as explained above.)

To check that the UV signal observed after •OH decay does not arise from the •OH but rather from the products, i.e., both H_2O_2 and $HO_2^{\bullet}/O_2^{\bullet-}$ radicals, we performed an experiment showing the time evolution of the spectrum at 350 °C. Figure 4 presents the result of this experiment. Proceeding from time zero after the electron pulse toward longer times, we observed a gradual decay of the spectrum. However, in the region of 310 nm we found almost complete decay of the band that is related to the gas-phase •OH radical absorption[43] (see Discussion below). This seems to confirm that the product absorption completely dominates by 10 μs.

The product absorption comes from one of the two mechanisms mentioned above. We tested both. Fitting reaction 2 with room-temperature hydrogen peroxide extinction coefficient required larger rate constants for •OH + H_2O_2 than one would expect from Arrhenius extrapolation of literature data.[42] That approach led to k_2 being almost 3 times higher than the extrapolation at 350 °C, and the temperature dependence in the entire experimental range deviated distinctly from the previous results.[42] On the other hand, forcing Arrhenius behavior of reaction 2 and allowing for peroxide absorbance adjustment led to roughly 3 times larger H_2O_2 extinction coefficient at 350 °C than at room temperature. This result is not impossible if the spectrum red-shifts, as was already discussed. (It has now also been pointed out to us that the gas-phase absorption of H_2O_2 increases with temperature in this wavelength region.[37]) For either explanation of the product absorption, the temperature dependence of reaction 1 was basically the same and the numbers shifted only 10−15%. From this exercise we conclude that we are able to achieve good estimation of the rate of the second-order decay of •OH radicals, but the experiment cannot deliver exact information about temperature changes of the rate coefficients for reaction 2.

It is worth noting that an additional obstacle comes from uncertainty in the sapphire transient absorption contribution at higher temperatures. As mentioned in the Experimental Section all the measurements in the SCW cell required subtraction of sapphire absorption signals. The signal amplitude from sapphire windows at longer times after the electron pulse increases dramatically with temperature, and at 350 °C it is comparable with the transient absorption signal amplitudes resulting from the irradiation of aqueous solutions. The comparison of sapphire absorptions at temperatures varying from 200 to 380 °C for two commercial sapphire windows is presented in the Supporting Information. One can expect that if the temperature of the sapphire windows in the empty cell differs enough from the temperature of the sapphire windows with the fluid in it (the thermocouple placed in the cell does not touch the window surface but rather the liquid phase in the center of the cell and indirectly the body of the metal cell), an error could result in the corrected residual absorption at longer times after the pulse of electrons. Therefore we exchanged sapphire windows and, instead of commercial synthetic sapphire windows (ESCO

Products), we used heat exchange method manufactured vacuum-UV-grade sapphire windows (HEM VUV sapphire, Crystal Systems) that were expected to have a lower level of both impurities and crystal defects.[44] In fact, the transient absorption profile of vacuum-UV-grade windows in the deep UV was much more convenient for transient absorption measurements at elevated temperatures (The comparison of the transient absorption signals of the two different types of sapphire windows at 350 °C is shown in Supporting Information along with some other data comparing the two types of windows). Where inexpensive commercial windows show increase of absorption after the pulse, the vacuum-UV-grade windows show a small bleaching with no apparent change in the transmittance level on the time scale of experiment. To compare how this difference affects our data at the highest temperatures, we performed a series of tests. The result of $^{\bullet}OH$ decay analysis at 300−350 °C showed that, by using either vacuum-UV-grade or commercial grade windows, we were able to obtain comparable results for k_1. However, signals related to the product formation, i.e., several microseconds after the electron pulse, differed enough to change by 100% the numbers for H_2O_2 ϵ or k_2 (depending on the fitting approach; see above) at 350 °C. We concluded once again that the level of confidence for the numbers reported for reaction 1 can be relatively high, but to avoid the problem of sapphire absorption, the vacuum-UV-grade sapphire windows should be used in the range 300−350 °C.

Ultimately, we could not determine from fitting whether the long-time absorption originates from H_2O_2 or the $HO_2^{\bullet}/O_2^{\bullet-}$ radical or both together. To settle the issue, we performed back-to-back experiments at 300 °C at neutral pH and at pH = 11 (i.e., 10^{-3} m NaOH) where we expected to see $O_2^{\bullet-}$ rather than $HO_2^{\bullet}$ in the case of reaction (2) dominance. The $O_2^{\bullet-}$ extinction coefficient at 250 nm is twice as large as that of $HO_2^{\bullet}$ [38]. The result of the experiment shows no change, to within 5%, in the product absorption after $^{\bullet}OH$ decay. It convinced us that the final absorption originates mainly from H_2O_2 at this temperature.

C. Fitting Model. Even though we were able to fit our data with a very simple model including only reactions 1 and 2, there are certainly other processes contributing to the kinetics, and the fitting parameters of the simple model may not give correct rate constants. We built a more extensive fitting model that accounts for all other reactions occurring during the water radiolysis as well as including all extinction coefficients for the other absorbing species present in the system. With extensive testing, we converged on the following list as the only significant processes in the N_2O-saturated water system on the time scale of interest:

$$^{\bullet}OH + {}^{\bullet}OH \rightarrow H_2O_2 \quad (1)$$

$$^{\bullet}OH + H_2O_2 \rightarrow HO_2^{\bullet} + H_2O \quad (2)$$

$$e^-_{aq} + N_2O + H_2O \rightarrow {}^{\bullet}OH + N_2 + OH^- \quad (5)$$

$$^{\bullet}OH + H^{\bullet} \rightarrow H_2O \quad (6)$$

$$HO_2^{\bullet} \leftrightarrow O_2^{\bullet-} + H^+ \quad (7)$$

$$H^{\bullet} + N_2O \rightarrow {}^{\bullet}OH + N_2 \quad (8)$$

The reaction 2 rate constants were extrapolated using the Arrhenius parameters determined previously by Christensen et. al[42] up to 150 °C. As explained above, the $HO_2^{\bullet}$ product makes little contribution to the final absorbance at high temperature, and our data are consistent with the Arrhenius extrapolation. Reaction 6 rate constants were calculated as by Elliot.[13,26] Reactions 7,−7 and 8 were estimated as described in our recent publication.[38] These reactions all represent minor corrections to the $^{\bullet}OH$ recombination kinetics. The extinction coefficients and G values were applied as stated above. For studying second-order decay of $^{\bullet}OH$ radicals, three doses were chosen for each temperature, varying from 11 to 70 Gy. Figure 3 presents the experimental data collected in N_2O saturated water at 250 nm with global fitting curves superimposed at two temperatures: 225 and 350 °C. Figure 5 shows a plot of the rate constant for reaction 1 studied in the range 150−350 °C. The new rate constants are summarized in Table 2. The data points shown represent an average of the fitted rate constants obtained for the set of fitting parameters varied within their accuracy limits at each temperature. The ±20% error bars are indicative of the range of rate constants obtained when the fit was "good", but this is a qualitative rather than a quantitative measure. The data below 200 °C were obtained by Elliot et al.[26] Our new measurements match quite well with the previous results, when the extinction coefficients are adjusted to common values. Above 200 °C, the rate constant stays basically on the same level around 1.2×10^{10} M^{-1} s^{-1}. The value of this rate constant at 350 °C was overestimated by a factor of 2.5 by the best previous extrapolations.[13]

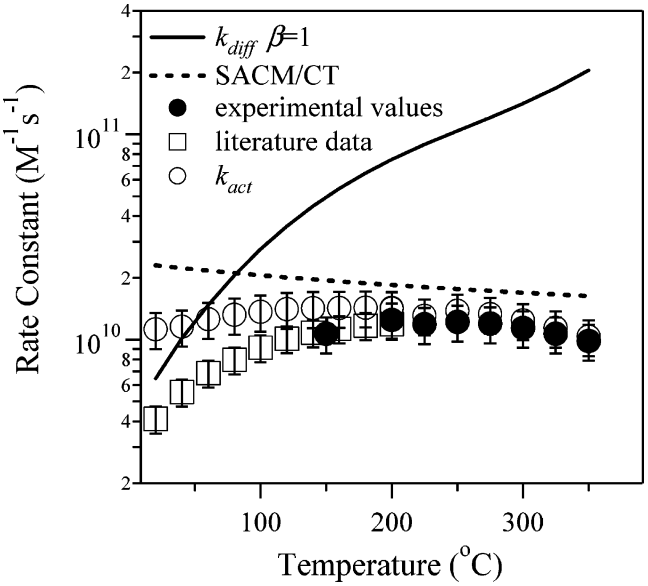

Figure 5. Temperature dependence of reaction 1 rate constants: (□) values reported by Elliot;[26] (●) experimental values from our studies; (---) SACM/CT limiting high-pressure gas-phase values reported by Troe and Ushakov;[57] (—) diffusion-limited rate constants calculated on the basis of the Smoluchowski equation with $\beta = 1$; (○) limiting k_{act} calculated on the basis of the Noyes eq 3 with use of given k_{diff} and k_{obs}.

TABLE 2: Fitted Rate Constants for Reaction (1)

temp (°C)	$k_3 \times 10^{-10}$ (M^{-1} s^{-1}) ± 20%
150	1.06
200	1.25
225	1.14
250	1.21
275	1.20
300	1.14
325	1.07
350	0.99

IV. Discussion

Although it was never our intention, we find that we have gathered significant new information on the UV absorption spectrum of •OH radical in water during the course of our study. We first review this subject and provide an interpretation of the spectrum changes consistent with our kinetics data. We then consider the new rate constant information for reaction 1 and make a connection with high-pressure gas-phase measurements.

•OH Radical Spectrum. At room temperature the •OH radical has a broad absorption band with a maximum around 230 nm and a long-wavelength tail that extends beyond 320 nm even out to 400 nm. Our result, shown in Figure 2, corresponds well to the results reported over the last 30 years.[9,33,35,45,46] As we were not able to extend our measurements below 230 nm at higher temperatures, we cannot discuss any changes in the band maximum[9] or the existence of an additional band described previously in the 188−200 nm region.[45] The most recent studies by Alam et. al[47] have shown no special features at 190−250 nm of the •OH radical spectrum, in contrast to the spectrum reported by Czapski et. al[35] and other researchers.[48] This discrepancy has been neither resolved nor discussed recently but is most likely explained by the larger spectral bandwidth (not reported in the paper) in Alam's experiment compared with the narrow bandwidth (0.95 nm) used earlier.[45] Nielsen et al. suggested this band below 200 nm was similar in origin to the H• atom absorption—a red shift of the water molecule absorption in the first solvation shell of the radical.[33] (Though it has not been noted in this context, a bound to unbound $^2\Pi \rightarrow {}^2\Sigma^-$ transition should also be found in the vacuum UV around 170 nm.[49])

The 230 nm band observed with •OH in liquid water is not found for •OH in the gas phase, which only has one near UV absorption band around 307 nm,[43,49,50] corresponding to a $^2\Pi \rightarrow {}^2\Sigma^+$ intramolecular transition. In crystalline H_2O ice two forms of •OH radical were reported. One was reported in the region above 200 nm very much like •OH dissolved in liquid H_2O and was believed to be hydrogen-bonded •OH (in a substitutional position),[51] and the other with maximum at 280 nm was believed to be •OH in "interstitial" positions.[52]

Treinin and Hayon argued that the apparent blue shift (1.4 eV) of the 230 nm band in water relative to the 307 nm band in vacuum is too large to be explained by a solvation effect.[53] They ascribe the •OH absorption at 230 nm to a charge-transfer transition involving H_2O as donor and •OH radical as acceptor, much like the H• atom absorption. Nielsen et al. disagreed with this assessment and noted a small isotope effect on the 230 nm band for •OH in H_2O relative to •OD in D_2O, whereas isotope shifts for H• atom vs D• atom and for solvated electron deep UV absorption in the two solvents are quite apparent.[33] These authors instead compared the •OH spectrum with the (0.8 eV) blue shift of the UV spectrum of H_2O on going from the vapor to liquid.[33] This disagreement over the origin of the •OH spectrum has apparently not been discussed further since that time.

Spectra have since been obtained at higher temperatures. In their very first paper about high-temperature pulse radiolysis, Christensen and Sehested reported •OH spectrum changes from 20 to 200 °C.[48] A decade later in their high-temperature analysis, Buxton and co-workers reported •OH[41] and •OD[54] spectra and claimed no significant changes with temperature. However, these published •OH radical spectra do show evidence of a change with temperature.[41] The spectra normalized at 250 nm very clearly[54] show temperature-related differences in the 310 nm region. Looking back again to Christensen and Sehested's[48] spectra, one can see changes at 310 nm showing up already at 90 °C, and becoming more pronounced at 150 °C. It is therefore no surprise that we were able to record this change as well.

By analogy with the band observed in the gas phase around 307 nm, and interstitial •OH in crystalline ice at 280 nm, the simplest conclusion is that the observed absorption at 310 nm is related to •OH radicals that are not hydrogen bonded, and the 230 nm band corresponds to hydrogen-bonded •OH. With increasing temperature the population of hydrogen-bonded •OH radicals should eventually decrease, and the 230 nm band should decrease as the 310 nm band increases. This is actually the case in our experiment, and it makes sense of our preliminary observation that the 250 nm extinction coefficient of •OH decreases at elevated temperature. Simple inspection of the spectra in Figure 2 then suggests that at 350 °C less than half of •OH radicals are hydrogen bonded! This is also the conclusion reached in a fully classical MD simulation of •OH in SPC/E water by Svishchev and Plugatyr.[55]

However, we still have the problem of the origin of the 230 nm band. We agree with Treinin and Hayon[53] that 1.4 eV is far too large a solvent shift for the intramolecular $^2\Pi \rightarrow {}^2\Sigma^+$ transition. The smaller but already very large 0.8 eV blue shift of the lowest water band has its origin in a ground-state to Rydberg transition, where a very large condensation effect is plausible. As for the claim there is no •OH/•OD isotope effect for the 230 nm band, this is not clearly supported by the published spectra. The comparison of spectra is made very difficult by overlapping bands in the deep UV, a difference in spectrum shapes, and possible absorbance by other transients. It makes more sense that the 230 nm band is a charge-transfer band of •OH radicals that are hydrogen bonded to water, and that the 310 nm band corresponds to •OH which is not hydrogen bonded. Then the question remains, where is the intramolecular $^2\Pi \rightarrow {}^2\Sigma^+$ absorbance for •OH that is hydrogen bonded to water? We suggest this is the origin of the weak long tail extending to 400 nm in the room-temperature spectrum.[35] Our experiments have not probed this spectral region, but we predict that the long tail will attenuate at higher temperature much like the 230 nm band.

The sudden increase in the initial deep UV absorption below 250 nm observed above 300 °C (one example is shown on Figure 4) is not explained by our hydrogen-bonding interpretation. However, it can be understood on the basis of three trends: (i) the H• atom yield increases in the range 300−350 °C by more than 60%; (ii) the H• atom spectrum, originating with water molecules in the solvation shell, can be expected to shift toward the red in the same manner as H_2O with the temperature;[56] (iii) the •OH radical room-temperature band observed at 180 nm could shift to the red in the same manner as the H• atom. It has been found that the H_2O UV absorption edge shifts by 0.5 eV from room temperature to 350 °C, corresponding to roughly a 20 nm red shift in the UV.[27] If we assume similar behavior for the H• atom, we estimate that at 350 °C and 230 nm, the extinction coefficient of H• atom would be 613 M^{-1} cm^{-1}. Comparing yields of H• and •OH at 350 °C and their extinction coefficients indicates that the initial absorption at 230 nm originates roughly 50% from the H• atom and 50% from •OH radicals. Using the shift of the H• atom spectrum by 20 nm to correct the apparent initial absorption spectrum of •OH radicals below 250 nm, we were able to recover a shape of the •OH spectrum at 350 °C that resembles very well the shape observed at lower temperatures. Nevertheless, kinetic experiments performed above 300 °C, among them measurements of the H• + O_2 reaction rates that are the subject of

another article,[38] lead us to the conclusion that a 0.5 eV shift of the H• atom spectrum is somewhat too high, as the fitting of kinetic traces indicates that its extinction coefficient at 230 nm cannot reach values larger than those of the •OH radical. This leads us to point (iii), that the absorption spectrum of •OH radicals changes not only in response to the hydrogen bonding but also because of a red shift of the third band below 200 nm, which could originate with the solvating water molecules.[45,53]

Another explanation for the deep UV result above 300 °C could simply be a distortion error related to the broad monochromator bandwidth used at 230 nm. This was not expected to affect the data at the time of experiment because the H• atom spectrum was not expected to contribute much at 230 nm. Further studies are clearly needed to clarify these spectrum changes in the deep UV.

The evident spectral changes of •OH radicals are reflected in the determination of •OH radical absorption at the wavelength of interest, i.e., 250 nm. The changes of extinction coefficient for 250 nm versus the temperature from our experimental data are presented in Figure 2 (inset). Given insufficient information about the H• atom spectrum, one might expect a systematic underestimation of the •OH extinction at 250 nm. In this eventuality, the rate constants obtained here will be lowered by at most 25% at 350 °C and deviate less than this at lower temperatures.

•OH Radical Recombination. Our reaction rate measurements fall within 20% of numbers reported previously up to 200 °C by Elliot et al.[26] When we correct the previous results for the •OH absorbance changes vs temperature as described above, we have an excellent match between the data sets. The Noyes eq 3 was used to correlate the previous data, assuming that the k_{act} rate constant follows an Arrhenius law.[13] Extrapolation of this fit does not match our experimental numbers above 200 °C. It seems somewhat surprising that the studied rate constant does not change above 200 °C and remains basically unchanged up to 350 °C.

We follow the previous approach[13] in estimating the diffusion limit for reaction 1 from the Smoluchowski equation, using relative diffusion coefficient $D = 4.6 \times 10^{-9}$ m^2 s^{-1} at room temperature, and scaling the temperature dependence by the ratio of T/viscosity. The reaction distance R is assumed to be 4.4 Å,[13] independent of temperature. (We note immediately that these estimates could be up to 25% off.) Isolated $^2\Pi$ •OH radical is characterized by a large spin−orbit splitting of 139 cm^{-1}, due to the orbital angular momentum about the internuclear axis.[50] Hydrogen bonding is expected to quench this angular momentum and the resulting spin−orbit coupling. However, the fluctuations of hydrogen bonding within liquid water probably result in a very fast and large modulation of the local magnetic field in the •OH radical; this can be expected to cause very fast spin relaxation within the radical encounter pair and justifies the use of a spin factor $\beta = 1$. In Figure 5 we plot the estimated diffusion limit along with the observed rate constants from this study and from the earlier study of Elliot et al.[26] Using the Noyes equation, we then deduce the rate constant k_{act}, which is plotted in Figure 5 as the open circles. The dashed line in Figure 5 represents the limiting high-pressure gas-phase values calculated by Troe and Ushakov.[21,57] One can see that the calculated k_{act} corresponds very well to the limiting high-pressure values, with nearly the same magnitude,and above 200 °C the same weakly negative temperature dependence. By tweaking the estimate of k_{diff} to a lower value, we could get nearly the same negative temperature coefficient over the whole temperature range.

In a preceding paper,[38] we reported a very similar result for reaction of H• atoms with O_2. Once the diffusion limit was accounted for using the Smoluchowski equation and the Noyes equation, an activated rate constant in "perfect" agreement with the gas-phase high-pressure limit was found. In that system, the result may be expected because both H• atom and O_2 are hydrophobic. The water solvent has very little effect on the intermolecular potential near the reaction "bottleneck" and simply acts as a very efficient "third body". (There is no barrier to reaction for approximately 45° approach of H• with respect to the O−O internuclear axis, but for other angles a substantial barrier is present.) In the present case the close agreement of gas-phase and aqueous-phase reaction rates is surprising. The gas-phase reaction path is expected to involve a metastable HO···HO hydrogen-bonded pair, with a transition state that involves rotation of the central H• atom out from between the O atoms. In liquid water we can expect •OH to be hydrogen bonded to water much of the time, and other angles of approach probably dominate. The good agreement indicated in Figure 5 means that the barrierless inner reaction channel for oxygen−oxygen approach dominates in both phases, and that this channel is not strongly perturbed by the water solvent.

The most surprising aspect of the comparison with the gas-phase result is the slightly negative temperature dependence of k_{act}, in apparent agreement with the gas-phase negative temperature coefficient. In the gas phase this behavior comes primarily from the statistical factor for $^2\Pi_{1/2}$ and $^2\Pi_{3/2}$ spin−orbit states of the •OH radical.[57] The spin−orbit splitting is 139 cm^{-1}, with $^2\Pi_{3/2}$ being lower in energy. The ground singlet state of H_2O_2 product correlates with a pair of separated $^2\Pi_{3/2}$ •OH radicals. At very low temperatures only $^2\Pi_{3/2}$ is populated, and $^1/_4$ of the collisions will correlate with the singlet ground state, the rest correlating with repulsive triplet excited states. At higher temperatures, $^2\Pi_{1/2}$ becomes populated, resulting in a larger percentage of nonreactive collisions. In the limit of $kT \gg 139$ cm^{-1}, the statistical factor will reach $^1/_{16}$. The negative temperature coefficient comes from this transition of the statistical factor between $^1/_4$ at very low temperature and $^1/_{16}$ at very high temperature.

How can the same statistical factor apply to the aqueous-phase reaction? If the •OH radical is hydrogen bonded, this should quench the orbital angular momentum, and the spin−orbit states $^2\Pi_{1/2}$ and $^2\Pi_{3/2}$ are no longer eigenstates of the potential. We have to expect that this is the situation in liquid water much of the time, in between brief moments when the hydrogen bond breaks and •OH exists as a freely rotating molecule. (The UV absorption spectrum discussed above suggests that such moments do occur, and are even very common at higher temperature and lower densities.) When the •OH radical breaks free of hydrogen bonds, the probability of forming $^2\Pi_{1/2}$ or $^2\Pi_{3/2}$ eigenstate is dictated by the Boltzmann factor for the given temperature. It would seem that the only way to get exactly the same temperature-dependent statistical factor for both gas- and aqueous-phase rate constants is if the reaction path involves breaking hydrogen bonds to both radicals, momentarily producing the $^2\Pi_{1/2}$ or $^2\Pi_{3/2}$ spin−orbit eigenstates of the free •OH. Note that this is consistent with $\beta = 1$ used above in the Smoluchowski equation, because essentially each re-collision of an encounter pair could give a new random pair of $^2\Pi_{1/2}$ or $^2\Pi_{3/2}$ states.

It seems just as likely that the weak negative temperature dependence in our data above 200 °C is due to other factors (not the least of which could be experimental error), producing a serendipitous resemblance to the gas-phase result. If the

reacting •OH radicals are hydrogen bonded to water, and orbital angular momentum is quenched, a statistical factor of $^1/_{16}$ (0.0625) would be expected for formation of the ground state singlet, independent of temperature. That is, by reducing spin−orbit splitting to a small average value, the aqueous system is always in the high-temperature limit. The gas-phase statistical factor in our experimental temperature range is approximately $^1/_{10}$. If we normalize our aqueous-phase results with the factor 1.6, they lie nearly on top of the high-pressure limit result, suggesting that reaction of $^2\Pi_{3/2}$ OH radicals on the ground state singlet surface occur with almost identical rate constants in water and the gas phase.

V. Conclusion

Pulse radiolysis of N_2O-saturated water combined with UV transient absorption detection has allowed determination of the rate for OH radical self-recombination up to 350 °C. The values of the rate constant are smaller than predicted previously in the 200−350 °C range and show no apparent change in this regime. The temperature behavior and magnitude of the rate constant are in excellent agreement with the gas-phase high-pressure limiting rate, suggesting very little perturbation of the reaction path by the water solvent. In fact, above 200 °C where the diffusion limit is unimportant, the only obvious effect of the water solvent is to modify the statistical ratio of $^2\Pi_{1/2}$ or $^2\Pi_{3/2}$ spin−orbit sublevels, and to act as a third body. This suggests that high-level ab initio results are perfectly adequate for prediction of OH radical recombination rates in the condensed phase.

In the course of the study new information on the OH radical UV absorption spectrum was obtained, showing a decrease in the primary band at 230 nm and growth of a weak band at 310 nm at elevated temperature, with isosbestic point near 305 nm. We interpret the 230 nm band as due to hydrogen-bonded OH, and the 310 nm band corresponding to "free" OH. At the same time we find the absorption spectra of the H• atom and H_2O_2 shift toward the visible.

Acknowledgment. We thank Dr. Sergey Chemerisov for maintaining and operating the linac accelerator used in this work. We especially thank Dr. Juergen Troe for sharing an unpublished manuscript concerning the reaction 1 gas-phase high-pressure limit, and Dr. Larry Harding for useful discussions concerning the relevant statistical factors. We thank Dr. Daniel Chipman for very useful discussions regarding the UV absorption of OH radical. Work at Argonne National Laboratory was performed under the auspices of the Office of Science, Division of Chemical Science, US-DOE under contract number W-31-109-ENG-38. Additional support has been provided by US-DOE NERI grant 02-060. The Notre Dame Radiation Laboratory is supported by the Office of Basic Energy Sciences at the United States Department of Energy. This is document number NDRL-4689 from the Notre Dame Radiation Laboratory.

Supporting Information Available: Five figures and an explanation of transient absorption observed in two sapphire window samples at elevated temperatures. This material is available free of charge via the Internet at http://pubs.acs.org.

References and Notes

(1) Haber, L. C.; Vandsburger, A. *Combust. Sci. Technol.* **2003**, *175*, 1859.

(2) Pignatello, J. J.; Oliveros, E.; MacKay, A. *Crit. Rev. Env. Sci. Technol.* **2006**, *36*, 1.

(3) Draganic, I. G.; Draganic, Z. D. *The Radiation Chemistry of Water*; Academic Press: New York, 1971.

(4) Gonzalez, M. G.; Oliveros, E.; Worner, M.; Braun, A. M. *J. Photochem. Photobiol. C* **2004**, *5*, 225.

(5) Adewuyi, Y. G. *Ind. Eng. Chem. Res.* **2001**, *40*, 4681.

(6) Baulch, D. L.; Bowman, C. T.; Cobos, C. J.; Cox, R. A.; Just, T.; Kerr, J. A.; Pilling, M. J.; Stocker, D.; Troe, J.; Tsang, W.; Walker, R. W.; Warnatz, J. *J. Phys. Chem. Ref. Data* **2005**, *34*, 757.

(7) Buxton, G. V.; Greenstock, C. L.; Helman, W. P.; Ross, A. B. *J. Phys. Chem. Ref. Data* **1988**, *17*, 513.

(8) Ervens, B.; Gligorovski, S.; Herrmann, H. *Phys. Chem. Chem. Phys.* **2003**, *5*, 1811.

(9) Herrmann, H. *Chem. Rev.* **2003**, *103*, 4691.

(10) von Sonntag, C. *Free-radical-induced DNA damage and its repair. A chemical perspective*; Springer: Heidelberg, 2006.

(11) Koshizuka, S.; Oka, Y. *Prog. Nucl. Energy* **1998**, *32*, 547.

(12) Oka, Y.; Koshizuka, S. *J. Atom. Eng. Soc. Jpn.* **2002**, *44*, 600.

(13) Elliot, A. J. Rate Constants and G-Values for the Simulation of the Radiolysis of Light Water over the Range 0−300 °C. AECL report 11073, 1994.

(14) Zellner, R.; Ewig, F.; Paschke, R.; Wagner, G. *J. Phys. Chem.* **1988**, *92*, 4184.

(15) Forster, R.; Frost, M.; Fulle, D.; Hamann, H. F.; Hippler, H.; Schlepegrell, A.; Troe, J. *J. Chem. Phys.* **1995**, *103*, 2949.

(16) Fulle, D.; Hamann, H. F.; Hippler, H.; Troe, J. *J. Chem. Phys.* **1996**, *105*, 1001.

(17) Brouwer, L.; Cobos, C. J.; Troe, J.; Dubal, H. R.; Crim, F. F. *J. Chem. Phys.* **1987**, *86*, 6171.

(18) Harding, L. B. *J. Phys. Chem.* **1989**, *93*, 8004.

(19) Harding, L. B. *J. Phys. Chem.* **1991**, *95*, 8653.

(20) Maergoiz, A. I.; Nikitin, E. E.; Troe, J. *J. Chem. Phys.* **1995**, *103*, 2083.

(21) Troe, J. *Chem. Rev.* **2003**, *103*, 4565.

(22) Noyes, R. M. *Prog. React. Kinet.* **1961**, *1*, 129.

(23) Pilling, M. J.; Seakins, P. W. *Reaction kinetics*; Oxford University Press: Oxford, U.K., 1995.

(24) Christensen, H.; Sehested, K. *Radiat. Phys. Chem.* **1981**, *18*, 723.

(25) Elliot, A. J. *Radiat. Phys. Chem.* **1989**, *34*, 753.

(26) Elliot, A. J.; McCracken, D. R.; Buxton, G. V.; Wood, N. D. *J. Chem. Soc., Faraday Trans.* **1990**, *86*, 1539.

(27) Marin, T. W.; Takahashi, K.; Bartels, D. M. *J. Chem. Phys.* **2006**, *125*, 104314.

(28) Cline, J.; Takahashi, K.; Marin, T. W.; Jonah, C. D.; Bartels, D. M. *J. Phys. Chem. A* **2002**, *106*, 12260.

(29) Marin, T. W.; Cline, J. A.; Takahashi, K.; Bartels, D. M.; Jonah, C. D. *J. Phys. Chem. A* **2002**, *106*, 12270.

(30) Takahashi, K.; Cline, J. A.; Bartels, D. M.; Jonah, C. D. *Rev. Sci. Instrum.* **2000**, *71*, 3345.

(31) Lin, M. Z.; Katsumura, Y.; Muroya, Y.; He, H.; Wu, G. Z.; Han, Z. H.; Miyazaki, T.; Kudo, H. *J. Phys. Chem. A* **2004**, *108*, 8287.

(32) Janik, D.; Janik, I.; Bartels, D. M. *Radiat. Res.* Manuscript in preparation.

(33) Nielsen, S. O.; Michael, B. D.; Hart, E. J. *J. Phys. Chem.* **1976**, *80*, 2482.

(34) Vaghjiani, G. L.; Ravishankara, A. R. *J. Geophys. Res. [Atmos.]* **1989**, *94*, 3487.

(35) Czapski, G.; Bielski, B. H. J. *Radiat. Phys. Chem.* **1993**, *41*, 503.

(36) Sehested, K.; Christensen, H. *Int. J. Radiat. Appl. Instrum. Pt. C: Radiat. Phys. Chem.* **1990**, *36*, 499.

(37) Kijewski, H.; Troe, J. *Helv. Chim. Acta* **1972**, *55*, 205.

(38) Janik, I.; Marin, T.; Jonah, C. D.; Bartels, D. M. *J. Phys. Chem. A* **2007**, *111*, 79.

(39) Christensen, H.; Sehested, K. *J. Phys. Chem.* **1988**, *92*, 3007.

(40) Bielski, B. H. J.; Cabelli, D. E.; Arudi, R. L.; Ross, A. B. *J. Phys. Chem. Ref. Data* **1985**, *14*, 1041.

(41) Elliot, A. J.; Buxton, G. V. *J. Chem. Soc., Faraday Trans.* **1992**, *88*, 2465.

(42) Christensen, H.; Sehested, K.; Corfitzen, H. *J. Phys. Chem.* **1982**, *86*, 1588.

(43) Pellerin, S.; Cormier, J. M.; Richard, F.; Musiol, K.; Chapelle, J. *J. Phys. D: Appl. Phys.* **1996**, *29*, 726.

(44) Khattak, C. P.; Schmid, F. *J. Cryst. Growth* **2001**, *225*, 572.

(45) Pagsberg, P.; Christensen, H.; Rabani, J.; Nilsson, G.; Fenger, J.; Nielsen, S. O. *J. Phys. Chem.* **1969**, *73*, 1029.

(46) Janata, E. *Proc. Ind. Acad. Sci., Chem. Sci.* **2002**, *114*, 731.

(47) Alam, M. S.; Kelm, M.; Rao, B. S. M.; Janata, E. *Radiat. Phys. Chem.* **2004**, *71*, 1087.

(48) Christensen, H.; Sehested, K. *Radiat. Phys. Chem.* **1980**, *16*, 183.
(49) Vandishoeck, E. F.; Dalgarno, A. *J. Chem. Phys.* **1983**, *79*, 873.
(50) Herzberg, G. *Molecular Spectra and Molecular Structure. I. Spectra of Diatomic Molecules*, 2nd ed.; van Nostrand: New York, 1950.
(51) Ghormley, J. A.; Hochanadel, C. J. *J. Phys. Chem.* **1971**, *75*, 40.
(52) Taub, I. A.; Eiben, K. *J. Chem. Phys.* **1968**, *49*, 2499.
(53) Treinin, A.; Hayon, E. *J. Am. Chem. Soc.* **1975**, *97*, 1716.
(54) Buxton, G. V.; Lynch, D. A.; Stuart, C. R. *J. Chem. Soc., Faraday Trans.* **1998**, *94*, 2379.
(55) Svishchev, I. M.; Plugatyr, A. Y. *J. Phys. Chem. B* **2005**, *109*, 4123.
(56) Marin, T. W.; Takahashi, K.; Bartels, D. M. *J. Chem. Phys.* **2006**, *125*, 104314.
(57) Troe, J.; Ushakov, V. G. *Phys. Chem. Chem. Phys.* Submitted for publication.